Article

Electrocatalytic Performance of Fuel Oxidation by PtTi Nanoparticles

Hideki Abe, Futoshi Matsumoto, Laif R. Alden, Scott C. Warren, Héctor D. Abruña, and Francis J. DiSalvo

J. Am. Chem. Soc., **2008**, 130 (16), 5452-5458 • DOI: 10.1021/ja075061c • Publication Date (Web): 28 March 2008

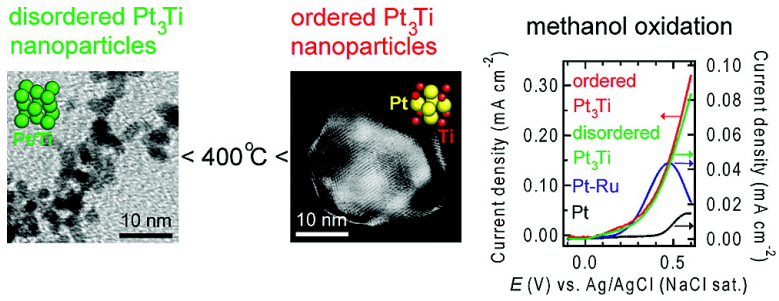

More About This Article

Additional resources and features associated with this article are available within the HTML version:

- Supporting Information
- Links to the 1 articles that cite this article, as of the time of this article download
- Access to high resolution figures
- Links to articles and content related to this article
- Copyright permission to reproduce figures and/or text from this article

View the Full Text HTML

J|A|C|S
ARTICLES

Published on Web 03/28/2008

Electrocatalytic Performance of Fuel Oxidation by Pt_3Ti Nanoparticles

Hideki Abe,*[,†,‡] Futoshi Matsumoto, Laif R. Alden,[§] Scott C. Warren, Héctor D. Abruña, and Francis J. DiSalvo*

Department of Chemistry and Chemical Biology, Baker Laboratory, Cornell University, Ithaca, New York 14853-1301, National Institute for Materials Science (NIMS), Sengen 1-2-1, Tsukuba, Ibaraki 305-0047, Japan, and Department of Chemistry, University of Pennsylvania, 231 South 34 Street, Philadelphia, Pennsylvania 19104-6323

Received July 9, 2007; E-mail: abe.hideki@nims.go.jp; fjd3@cornell.edu

Abstract: A Pt-based electrocatalyst for direct fuel cells, Pt_3Ti, has been prepared in the form of nanoparticles. Pt(1,5-cyclooctadiene)Cl_2 and Ti(tetrahydrofuran)$_2Cl_4$ are reduced by sodium naphthalide in tetrahydrofuran to form atomically disordered Pt_3Ti nanoparticles (FCC-type structure: $Fm\bar{3}m$; $a = 0.39$ nm; particle size $= 3 \pm 0.4$ nm). These atomically disordered Pt_3Ti nanoparticles are transformed to larger atomically ordered Pt_3Ti nanoparticles (Cu_3Au-type structure: $Pm\bar{3}m$; $a = 0.3898$ nm; particle size $= 37 \pm 23$ nm) by annealing above 400 °C. Both atomically disordered and ordered Pt_3Ti nanoparticles show lower onset potentials for the oxidation of formic acid and methanol than either pure Pt or Pt−Ru nanoparticles. Both atomically disordered and ordered Pt_3Ti nanoparticles show a much lower affinity for CO adsorption than either pure Pt or Pt−Ru nanoparticles. Atomically ordered Pt_3Ti nanoparticles show higher oxidation current densities for both formic acid and methanol than pure Pt, Pt−Ru, or atomically disordered Pt_3Ti nanoparticles. Pt_3Ti nanoparticles, in particular the atomically ordered materials, have promise as anode catalysts for direct fuel cells.

Introduction

There is a growing need for direct fuel cells operating near room temperature.[1,2] Direct fuel cells require anode catalysts that enable the direct conversion of chemical energy to electricity through the complete electrocatalytic oxidation of the fuels. Pure Pt is an excellent anode catalyst for the oxidation of clean hydrogen. However, pure Pt is not useful in practical direct fuel cells using carbon-containing fuels. The surface of pure Pt is highly susceptible to poisoning by CO, which is a reaction intermediate in the oxidation pathway of carbon-containing fuels. A Pt-based alloy electrocatalyst, Pt−Ru, is the current standard for the oxidation of carbon-containing fuels. Pt−Ru is more tolerant to CO poisoning and shows lower onset potentials for fuel oxidation than pure Pt.[3–5] The electrocatalytic performance of Pt−Ru, however, tends to decay with use due to the migration of the surface Ru atoms into bulk. Ru itself can also be leached out of the Pt−Ru by oxidation of the Ru, if the anode potential becomes too positive during power transients.

Recently, the authors and their collaborators have reported that high-performance electrocatalysts can be obtained in the family of Pt-based ordered intermetallic compounds.[6–8] Indeed, two of these ordered intermetallic compounds, PtBi and PtPb, show not only a higher tolerance to CO poisoning but also superior electrocatalytic activity toward formic acid oxidation than pure Pt, Pt−Ru, or Pd.[6–13] The discovery that PtBi and PtPb have a high impurity tolerance has prompted further searches for ordered intermetallic electrocatalysts that have high activity for the complete oxidation of methanol or even ethanol, which are more energetic fuels than formic acid.

Pt-based intermetallic compounds containing early *d*-metal elements, such as Pt_3Ti, have attracted attention for their interesting thermochemical properties. The enthalpy of formation of Pt_3Ti, $\Delta H_f = -298$ (kJ/mol of Ti), is one of the largest values

[†] Cornell University.
[‡] National Institute for Materials Science (NIMS).
[§] University of Pennsylvania.

(1) Reddington, E.; Sapienza, A.; Gurau, B.; Viswanathan, R.; Suranga-pani, S.; Somtkin, E. S.; Mallouk, T. E. *Science* **1998**, *280*, 1735–1737.
(2) Parsons, R.; VanderNoot, T. J. *Electroanal. Chem.* **1988**, *257*, 9–45.
(3) Long, J. W.; Stround, R. M.; Swider-Lyons, K. E.; Rolison, D. R. *J. Phys. Chem. B* **2000**, *104*, 9772–9776.
(4) Schmidt, T. J.; Gasteiger, H. A.; Behm, R. J. *J. Electrochem. Soc.* **1999**, *146*, 1296–1304.
(5) Costamanga, P.; Srinivisan, S. J. *Power Sources* **2001**, *102*, 242–252.
(6) Casado-Rivera, E.; Gál, Z.; Angelo, A. C. D.; Lind, C.; DiSalvo, F. J.; Abruña, H. D. *Chem. Phys. Chem.* **2003**, *4*, 193–199.
(7) Casado-Rivera, E.; Volpe, D. J.; Alden, L. R.; Lind, C.; Downie, C.; Vázquez-Alvarez, T.; Angelo, A. C. D.; DiSalvo, F. J.; Abruña, H. D. *J. Am. Chem. Soc.* **2004**, *126*, 4043–4049.
(8) Volpe, D. J.; Casado-Rivera, E.; Alden, L. R.; Lind, C.; Hagerdon, K.; Downie, C.; Korzeniewski, C.; DiSalvo, F. J.; Abruña, H. D. *J. Electrochem. Soc.* **2004**, *151*, A971–A977.
(9) Roychowdhury, C.; Matsumoto, F.; Mutolo, P. F.; Abruña, H. D.; DiSalvo, F. J. *Chem. Mater.* **2005**, *17*, 5871–5876.
(10) Roychowdhury, C.; Matsumoto, F.; Zeldovich, V.; Warren, S. C.; Mutolo, P. F.; Ballesteros, M.; Wiesner, U.; Abruña, H. D.; DiSalvo, F. J. *Chem. Mater.* **2006**, *18*, 3365–3372.
(11) Alden, L. R.; Han, D. K.; Matsumoto, F.; Abruña, H. D.; DiSalvo, F. J. *Chem. Mater.* **2006**, *18*, 5591–5596.
(12) Alden, L. R.; Roychowdhury, C.; Matsumoto, F.; Han, D. K.; Zeldovich, V.; Abruña, H. D.; DiSalvo, F. J. *Langmuir* **2006**, *22*, 10465–10471.
(13) Matsumoto, F.; Roychowdhury, C.; DiSalvo, F. J.; Abruña, H. D. Accepted by *J. Electrochem. Soc.*

 10.1021/ja075061c CCC: $40.75

found among the family of intermetallic compounds.[14] In contrast, the enthalpy of formation of Pt−Ru is only a few kJ/mol of Ru. In addition, the adsorption energy of CO to the Pt_3Ti surface is 20% smaller than that on a pure Pt surface, suggesting that Pt_3Ti might have a higher tolerance to CO poisoning than pure Pt.[15–17] In this work, we show that Pt_3Ti can be prepared in the form of nanoparticles and compare its electrocatalytic performance directly with that of conventional anode catalysts, including pure Pt nanoparticles and Pt−Ru nanoparticles.

The chemical coreduction of metal precursors in solvents is a popular strategy that has been applied to the synthesis of many kinds of intermetallic nanoparticles.[9–13,18–25] However, Ti-based intermetallic nanoparticles have not been synthesized so far by the coreduction strategy because Ti metal (zerovalent Ti) is extremely oxyphilic, especially when in the form of fine particles.[26] In order to prepare Pt_3Ti nanoparticles, we use air-free synthetic conditions involving an inert atmosphere and aprotic solvents. We use organometallic chlorides as metal precursors and a sodium-based reducing agent.[23–25]

The coreduction of Pt(1,5-cyclooctadiene)Cl_2 and Ti(tetrahydrofuran)$_2Cl_4$ by sodium naphthalide in tetrahydrofuran indeed leads to the formation of atomically disordered Pt−Ti nanoparticles (FCC-type structure: $Fm\bar{3}m$; $a = 0.39$ nm; particle size $= 3 \pm 0.4$ nm). These Pt−Ti nanoparticles grow in size upon annealing in vacuum. Atomically ordered Pt_3Ti nanoparticles (Cu_3Au-type structure: $Pm\bar{3}m$; $a = 0.3898$ nm; particle size $= 37 \pm 23$ nm) are obtained when annealed at temperatures up to 600 °C. Both atomically disordered and ordered Pt_3Ti nanoparticles show lower onset potentials for the oxidation of both formic acid and methanol than either pure Pt or Pt−Ru nanoparticles. Both types of Pt_3Ti nanoparticles show a much lower affinity toward CO adsorption than either pure Pt or Pt−Ru nanoparticles. Atomically ordered Pt_3Ti nanoparticles show substantially higher current densities in the oxidation of formic acid and methanol than atomically disordered Pt_3Ti, pure Pt, or Pt−Ru nanoparticles.

Experimental Section

Synthetic Methods. The organometallic precursor for Pt, Pt(1,5-cyclooctadiene)Cl_2 (99% purity), was used as purchased from STREM Chemicals Inc. The precursor for Ti, Ti(tetrahydrofuran)$_2Cl_4$, was synthesized from $TiCl_4$ (Aldrich; 99.9% purity) and distilled tetrahydrofuran (Fisher) according to literature procedures.[27] Precursor solutions containing different mole percentages of Ti(tetrahydrofuran)$_2Cl_4$ were prepared by dissolving 0.06 mmol (22.45 mg) of Pt(1,5-cyclooctadiene)Cl_2 and $0.06x/(100 - x)$ mmol of Ti(tetrahydrofuran)$_2Cl_4$ ($x \leq 80$) in 10 mL of distilled tetrahydrofuran (Fisher) under a dry Ar atmosphere. The precursor solutions were then transferred into a syringe.

Again under a dry Ar atmosphere, either 0.5 ($x \leq 25$) or $0.24 + 0.48x/(100 - x)$ ($25 < x \leq 80$) mmol each of sodium metal (Aldrich) and naphthaline (Fisher) were added into a two-neck flask containing 50 mL of distilled tetrahydrofuran (Fisher). One of the two necks of the flask was capped with a rubber septum. A dark-green solution of sodium naphthalide was obtained by stirring the solution overnight at room temperature under a dry Ar atmosphere.

The precursor solution was injected through the septum into the two-neck flask containing the stirred sodium naphthalide solution. The sodium naphthalide solution turned dark brown immediately upon injection. After stirring overnight, the solvent was distilled off at a reduced pressure to leave a dark-brown precipitate. The precipitate was washed with hexanes and methanol in sequence to remove byproducts, such as naphthaline and NaCl, again under a dry Ar atmosphere. After each washing step, the precipitate was separated from the washing solvent by centrifugation without air exposure. The final precipitates were dried by evacuation at room temperature. The products were air-stable, black powders. In the case of $x = 50$, the average mass of the product was 8.7 mg. The yield of the reaction is calculated to be 60% by dividing the mass of the product by the net masses of 0.06 mmol each of Pt and Ti contained in the precursor.

Characterization. Powder X-ray diffraction (*p*XRD; Scintag XDS 2000; Cu Kα radiation ($\lambda = 0.15418$ nm)) was performed for structural characterization. An ultrahigh vacuum scanning transmission electron microscope (UHV-STEM; VG HB501UX) was used for the microscopic observation of the morphology and particle sizes of the products. Specimens for UHV-STEM were prepared by dipping commercial sample holders for transmission electron microscopy (TEM) into the methanol suspensions of the products. The specimens for UHV-STEM were thoroughly dried by evacuation prior to observation. Structural analysis was performed using the UHV-STEM in the convergent beam electron diffraction (CBED) mode. The chemical composition of the product was evaluated using an energy dispersive spectroscopy (EDS) system attached to the UHV-STEM. The specific surface area of the product was determined with the Brunauer–Emmett–Teller (BET) method. A Micromeritics ASAP 2020 was used to collect a partial adsorption isotherm at liquid nitrogen temperature (−196 °C), with krypton as the adsorption gas.

Electrochemical Measurements. A 4 mg amount of the product was suspended in a mixture of 3.98 mL of distilled water (18 MΩ cm; Millipore Milli-Q), 1 mL of isopropyl alcohol, and 20 μL of a 5% w/w alcoholic solution of Nafion (Aldrich; EW: 1100). Suspensions of pure Pt nanoparticles (Johnson Matthey; HiSPEC-1000; ADS = 2–3 nm; surface area = 27 $m^2\ g^{-1}$) and Pt−Ru nanoparticles (Johnson Matthey; HiSPEC-6000, 1:1 a/o Pt/Ru, specific surface area = 70 $m^2\ g^{-1}$) were prepared in the same way. Using a spin-coater, each of the resultant suspensions was spread and dried to form a film on the polished surface of a glassy carbon (GC) electrode with a diameter of 3 mm. Each of the films contained 70 $\mu g\ cm^{-2}$ of the catalysts. Prior to cyclic voltammetry (CV) and CO stripping measurements, the film containing the products was pretreated in a 0.1 M sulfuric acid solution for 30 min by applying a DC potential of −0.7 V. Both the film containing pure Pt nanoparticles and that containing Pt−Ru nanoparticles were pretreated in a 0.1 M sulfuric acid solution by sweeping the potential between −0.2 and 0.2 V 10 times at a sweep rate of 10 mV s^{-1}.

CV measurements were performed at a sweep rate of 10 mV s^{-1} in Millipore-water solutions of 0.1 M sulfuric acid (Sigma-Aldrich; 99.999% purity) that contained 0.5 M of fuel materials: formic acid (Mallinckrodt; 88% analytical reagent) or methanol (Burdick and Johnson; 99.9% purity). The GC electrodes were rotated at 2000 rpm during CV measurements to suppress the formation of gas bubbles on the electrode surface. CO stripping measurements were performed in a Millipore-water solution of 0.1

(14) Meschter, P. J.; Worrell, W. L. *Met. Trans.* **1976**, *7A*, 299–305.
(15) Bardi, U.; Somorjai, G. A.; Ross, P. N. *J. Catal.* **1984**, *85*, 272–276.
(16) Bardi, U.; Dahlgren, D.; Ross, P. N. *J. Catal.* **1986**, *100*, 196–209.
(17) Ross, P. N. *Electrochim. Acta* **1991**, *36*, 2053–2062.
(18) Sra, A. K.; Schaak, R. E. *J. Am. Chem. Soc.* **2004**, *126*, 6667–6672.
(19) Schaak, R. E.; Sra, A. K.; Leonard, B. M.; Cable, R. E.; Bauer, J. C.; Han, Y.-F.; Means, J.; Teizer, V.; Vasquez, Y.; Funck, E. S. *J. Am. Chem. Soc.* **2005**, *127*, 3506–3515.
(20) Leonard, B. M.; Bhuvanesh, N. S. P.; Schaak, R. E. *J. Am. Chem. Soc.* **2005**, *127*, 7326–7327.
(21) Sra, A. K.; Ewers, T. D.; Schaak, R. E. *Chem. Mater.* **2005**, *17*, 758–766.
(22) Cable, R. E.; Schaak, R. E. *Chem. Mater.* **2005**, *17*, 6835–6841.
(23) Baldwin, R. K.; Pettigrew, K. A.; Ratai, E.; Augustine, M. P.; Kauzlarich, S. M. *Chem. Commun.* **2002**, *17*, 1822–1823.
(24) Chiu, H. W.; Chervin, C. N.; Kauzlarich, S. M. *Chem. Mater.* **2005**, *17*, 4858–4864.
(25) Chiu, H. W.; Kauzlarich, S. M. *Chem. Mater.* **2006**, *18*, 1023–1028.
(26) Tsai, K. L.; Dye, J. L. *J. Am. Chem. Soc.* **1991**, *113*, 1650–1652.
(27) *Inorganic Synthesis*, Vol. XXI; Fackler, J. P., Eds.; Wiley and Sons: New York, 1982; pp 135–140..

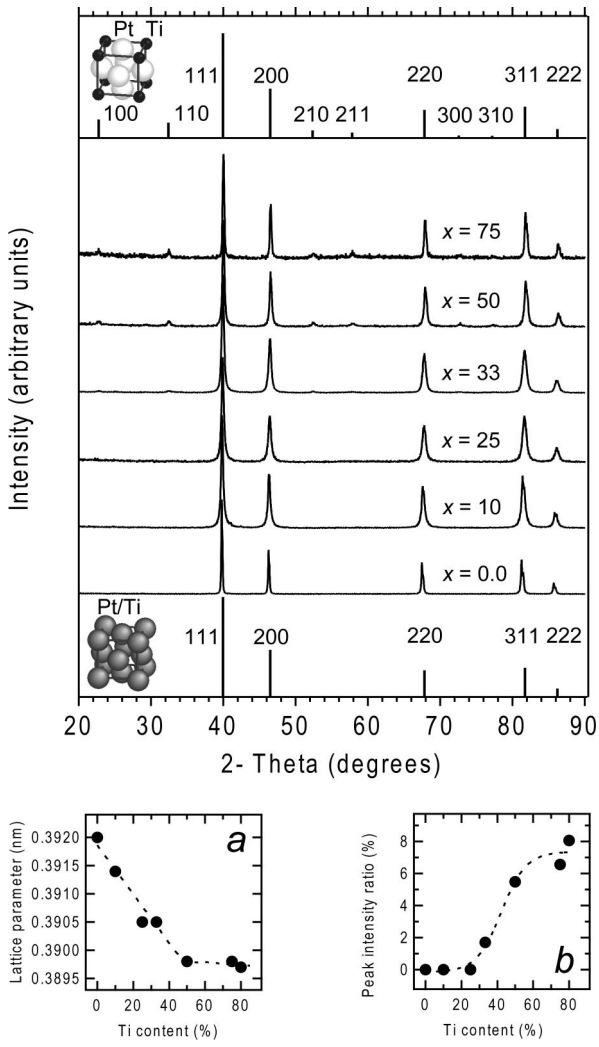

Figure 1. *p*XRD profiles of the products with different stoichiometries and annealed at 600 °C. Simulated *p*XRD peaks for the disordered FCC-type and the ordered Cu_3Au-type structures are indicated by solid markers at the bottom and the top of the figure, respectively, together with the corresponding structural models. Insets *a* and *b* show the lattice parameter and the peak ratio between the 110 and 111 reflections, respectively, as functions of the Ti content in the precursors.

M sulfuric acid. The solution was deaerated with a dry N_2 gas for 30 min prior to the measurements. The sulfuric acid solution was then bubbled with CO gas (99.9% purity) for 30 min and again with a dry N_2 gas for 30 min while the electrode potential was held at −0.12 V. CO stripping measurements were carried out at a sweep rate of 10 mV s^{-1} in the potential range between −0.2 and 0.65 V under a dry N_2 atmosphere. The electrode potentials for both CV and CO stripping measurements were referenced to a sodium chloride saturated Ag/AgCl electrode without regard for the liquid junction.

Results and Discussion

Figure 1 shows the *p*XRD patterns for the products prepared from the precursors containing increasing amounts, *x*, of Ti(tetrahydrofuran)$_2$Cl$_4$. The products were annealed at 600 °C for 12 h in vacuum prior to *p*XRD measurements. The *p*XRD for the product prepared at $x = 0$ shows five peaks at 39.8°, 46.3°, 67.5°, 81.3°, and 85.7°. The product is easily identified as pure Pt, since the *p*XRD peaks are consistent with the 111, 200, 220, 311, and 222 reflections of pure Pt (FCC-type structure: $Fm\bar{3}m$; $a = 0.3920$ nm), respectively.[28]

The *p*XRD patterns of the products prepared in the range $0.0 \leq x < 33$ are ascribed to the same FCC-type structure. The *p*XRD peaks slightly shift to higher angles relative to those of pure Pt, which shows that the lattice constant decreases with increasing in *x* (inset *a*). This contraction in the lattice parameter indicates that the Pt matrix incorporates at least some Ti with increasing *x*. We conclude that the products, therefore, are an "alloy" of Pt and Ti, in which Pt and Ti are distributed over the FCC sites (see the simulated *p*XRD pattern and the structural model at the bottom of Figure 1).

In the range $33 \leq x < 50$, six additional peaks become visible at 22.8°, 32.4°, 52.5°, 57.8°, 72.6°, and 77.4°. These peaks are assigned to the 100, 110, 210, 211, 300, and 310 reflections of the Cu_3Au-type structure ($Pm\bar{3}m$; $a = 0.39$ nm; see the simulated *p*XRD pattern and the structural model at the top of Figure 1), respectively. The relative intensity of the 110 peak to the 111 peak increases with increasing *x*, which shows that full ordering in the Cu_3Au-type structure is developing with increasing *x* (inset *b*). The lattice parameter of the product, however, remains larger than that of stoichiometric Pt_3Ti, $a = 0.3898$ nm (inset *a*).[28] This indicates that the Ti content of the product is still low relative to the stoichiometry of Pt_3Ti, even when the reactants are mixed in the range $33 < x < 50$.

The *p*XRD patterns of the products show a good fit with the stoichiometric Pt_3Ti with the Cu_3Au-type structure in the range $x \geq 50$ ($Pm\bar{3}m$; $a = 0.3898$ nm). Both the lattice parameter and the relative intensity of the 110 to 111 peaks are virtually independent of *x* over this range (insets *a* and *b*). This indicates that the products prepared in the range $x \geq 50$ are, regardless of *x*, stoichiometric Pt_3Ti that is fully ordered in the Cu_3Au-type structure. The lowest content of Ti(tetrahydrofuran)$_2$Cl$_4$ in the precursor to obtain stoichiometric Pt_3Ti is, therefore, $x = 50$. The precursor solution with the composition of $x = 50$ contains an excess of Ti relative to the stoichiometry of Pt_3Ti and corresponds to the known phase PtTi. We surmise that the excess Ti is leached out of the products when washing with methanol, by forming titanium methoxide. Indeed, a Ti-containing gel precipitates when the methanol supernatant is exposed to air and/or mixed with water. *p*XRD showed that the precipitate is converted into a mixture of titanates of $Na_yTiO_{2-y/2}$ by firing in air at 1000 °C. The Na presumably comes from the other byproduct, NaCl.

Figure 2 shows *p*XRD patterns for the products prepared from the precursor with a composition of $x = 50$. The products, excluding the as-prepared one, were annealed at different temperatures up to 600 °C for 12 h in vacuum prior to *p*XRD. The *p*XRD for the as-prepared product shows four broad peaks centered near 40°, 46°, 68°, and 82°. The observed *p*XRD pattern is consistent with the *p*XRD patterns for either the disordered FCC-type structure ($Fm\bar{3}m$; $a = 0.39$ nm; see the simulated *p*XRD pattern at the bottom of Figure 2) or the ordered Cu_3Au-type structure (see the simulated *p*XRD pattern at the top of Figure 2) with a domain size of approximately 3 nm. The four broad peaks are assigned to the 111, 200, 220, and 311 reflections, respectively. The crystal structure of the as-prepared product is not determined solely on the basis of *p*XRD, since the weak ordering peaks of the Cu_3Au-type

(28) *Pearson's Handbook of Crystallographic Data for Intermetallic Phases*, Vol. 3; Villars, P. L., Calvert, L. D., Eds.; American Society for Metals: Metals Park, OH, USA, 1985; pp 3044, 3058, 3059.

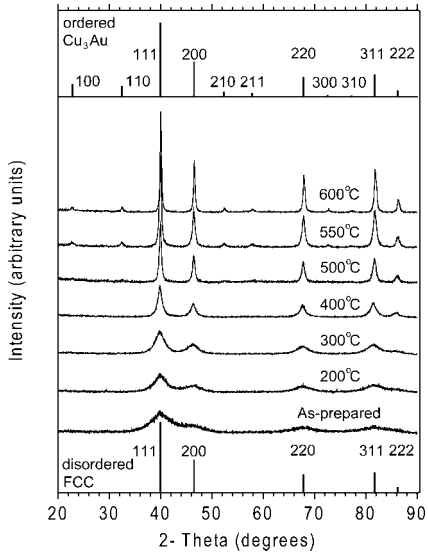

Figure 2. *p*XRD profiles of the products annealed in vacuum at various temperatures. Simulated *p*XRD peaks for the disordered FCC-type and the ordered Cu_3Au-type structures are indicated by solid markers at the bottom and the top of the figure, respectively.

structure would not be visible when broadened as much as the more intense peaks. The as-prepared product is clearly not PtTi, even though the stoichiometry of the precursor solution is Pt/Ti = 1:1. PtTi adopts the AuCd-type structure (*Pmma*; a = 0.4592, b = 0.2761, and c = 0.4838 nm), which gives a *p*XRD pattern that is very different from the ones observed here.[28]

Annealing at 200 and 300 °C for 12 h results in some sharpening of the 111, 200, 220, and 311 peaks, due to grain growth. When the annealing temperature is 400 °C, the 222 peak begins to be visible at 86°. Additional peaks appear at 22.7°, 32.4°, and 52.4° and beyond when the annealing temperature exceeds 500 °C. The *p*XRD for the product annealed above 550 °C shows six weak peaks at 22.7°, 32.4°, 52.4°, 57.9°, 72.8°, and 77.4°. These peaks are assigned to the 100, 110, 210, 211, 300, and 310 ordering reflections of Pt_3Ti in the Cu_3Au structure-type ($Pm\bar{3}m$; a = 0.3898 nm; see the simulated *p*XRD pattern at the top of Figure 2). It is clear that the stoichiometry of the product annealed at 600 °C is close to Pt/Ti = 3:1, since the observed *p*XRD pattern has a good fit with that of stoichiometric Pt_3Ti with a domain size of 35 nm.

Microscopic experiments using UHV-STEM were performed on the as-prepared product and the product annealed at 600 °C. Figure 3*a* shows a UHV-STEM image of the as-prepared product. Ellipsoidal nanoparticles with an average size of 3.0 ± 0.4 nm aggregate to form clusters (Figure 3*a*). The individual nanoparticles are mostly single crystal particles, since the particle size is roughly consistent with the domain size evaluated from the *p*XRD data, 3 nm. Figure 3*b* shows a CBED pattern of the nanoparticle indicated by an arrow in the inset. The zone axis is assigned to one of the <111> axes of the cubic lattice, since the observed spots show nearly 6-fold symmetry. The CBED spots nearest the 000 reflection are indexed by the {220} reflections of either the disordered FCC-type or the ordered Cu_3Au-type structures, as expected from *p*XRD. Although the {220} reflections are reasonably sharp and strong, the {110} ordering reflections corresponding to the ordered Cu_3Au-type structure are not visible. This shows that the nanoparticle is not atomically ordered in the Cu_3Au-type structure. The ordering reflections of the ordered Cu_3Au-type structure were not visible

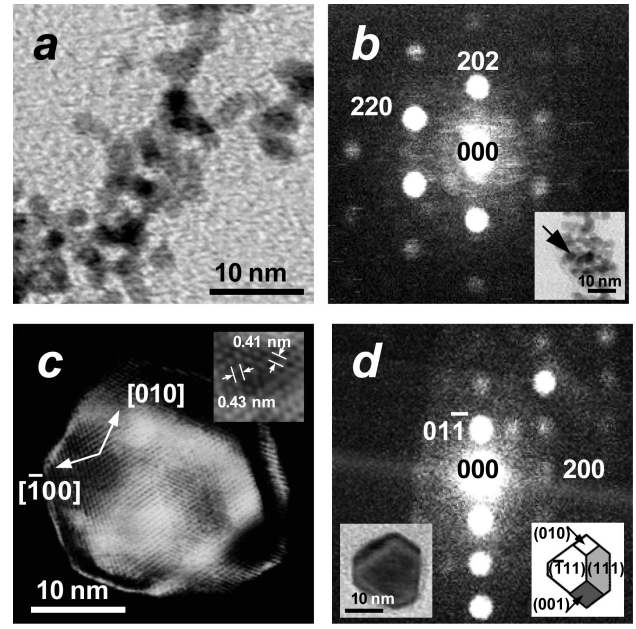

Figure 3. *a*. STEM image of the as-prepared product. *b*. CBED pattern of the nanoparticle indicated in the inset by an arrow. *c*. STEM image of a Pt_3Ti nanoparticle in the product annealed at 600 °C. The inset shows an atomic-resolution STEM image. *d*. CBED pattern of a Pt_3Ti nanoparticle in the product annealed at 600 °C. The left inset shows a STEM image of the Pt_3Ti nanoparticle corresponding to the CBED pattern. The right inset shows a model of the outer shape of the Pt_3Ti nanoparticle shown in the left inset.

in any of the CBED patterns of nanoparticles in the as-prepared product. We conclude on the basis of CBED and *p*XRD that the as-prepared product consists of atomically disordered Pt−Ti nanoparticles with the FCC-type structure.

In contrast to the as-prepared product, the product annealed at 600 °C consists of well-dispersed polyhedral nanoparticles with a size of 37 ± 23 nm (Figure 3*c*). The average particle size is roughly consistent with the domain size evaluated from *p*XRD, 35 nm. Two kinds of lattice fringes are observed perpendicular to the [100] or [010] axes of this particular nanoparticle. The intervals of the lattice fringes perpendicular to the [100] and [010] axes are 0.43 and 0.41 nm, respectively (inset of Figure 3*c*). Both are within measurement errors of the *d*-spacing of the {100} planes of Pt_3Ti with the Cu_3Au-type structure, 0.3898 nm. Figure 3*d* is a CBED pattern obtained with the incident electron beam nearly perpendicular to the hexagonal face of the nanoparticle shown in the left inset. All the CBED spots are indexed on the basis of the Cu_3Au-type structure ($Pm\bar{3}m$; a = 0.3898 nm). This indicates that the product annealed at 600 °C consists of atomically ordered Pt_3Ti nanoparticles with the Cu_3Au-type structure, as expected from *p*XRD. A morphological model of that atomically ordered Pt_3Ti nanoparticle is presented in the right inset.

Figure 4 shows the EDS profiles of the atomically disordered Pt−Ti nanoparticle and the atomically ordered Pt_3Ti nanoparticle corresponding to the insets of Figures 3*b* and 3*d*, respectively. Both types of nanoparticles are confirmed to be composed of Pt and Ti, since all the EDS peaks are assigned to Pt or Ti except for the Cu signals from the sample holder. Light elements, such as carbon, are not separately determined in the specimen because the TEM sample holder has a thin carbon film to support the nanoparticles. The stoichiometries of the atomically disordered Pt−Ti nanoparticles and atomically ordered Pt_3Ti nanoparticles were evaluated to be Pt/Ti = 64:35 (±15) and 77:22 (±3),

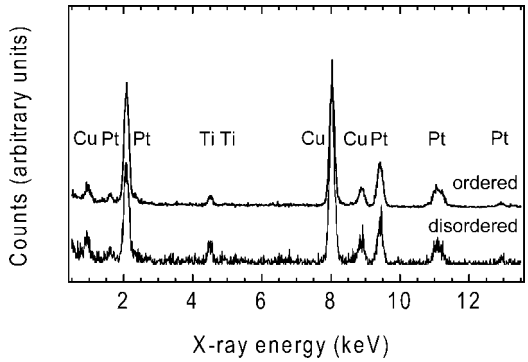

Figure 4. EDS profiles of the atomically disordered Pt−Ti and atomically ordered Pt_3Ti nanoparticles corresponding to the insets of Figure 3b and 3d, respectively.

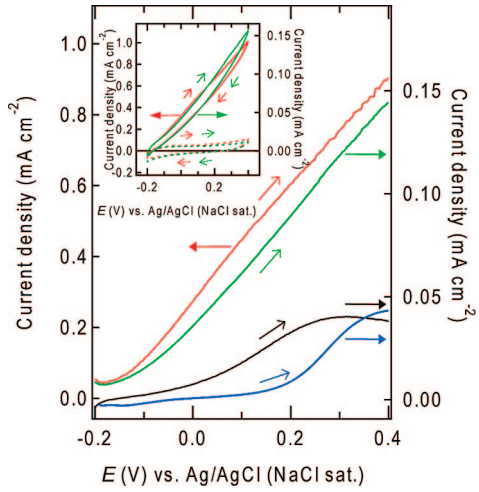

Figure 5. Full curves in the inset represent the CV profiles of atomically disordered (green) and ordered (red) Pt_3Ti nanoparticles for formic acid oxidation. Dashed curves in the inset represent the profiles of the blank test for atomically disordered (green) and ordered (red) Pt_3Ti nanoparticles. The green and red curves correspond to the right and left axes of the inset, respectively. The green, red, black, and blue curves on the main panel represent the intrinsic current densities of atomically disordered Pt_3Ti, atomically ordered Pt_3Ti, pure Pt, and Pt−Ru nanoparticles, respectively, for the oxidation of formic acid.

respectively, by semiquantitative EDS analysis of the randomly sampled nanoparticles. Neither data set is corrected for sample thickness. The large error bars obtained for the atomically disordered Pt−Ti nanoparticles arise from the low signal-to-noise due to small sample volumes but might also be consistent with a broad range of stoichiometries, from 3:1 to 1:1 for Pt/Ti. We describe the atomically disordered Pt−Ti nanoparticles as "atomically disordered Pt_3Ti nanoparticles" for brevity. In contrast, it is clear that the atomically ordered Pt_3Ti nanoparticles are an "intermetallic compound" with a well-defined 3:1 stoichiometry.

CV and CO stripping measurements were performed on both atomically disordered and ordered Pt_3Ti nanoparticles. The measured currents were converted into current densities using the specific surface areas of atomically disordered and ordered Pt_3Ti nanoparticles, $(1.1 \pm 0.1) \times 10^2$ and 9.2 ± 5.7 m^2 g^{-1}, respectively, on the basis of the average particle sizes evaluated by STEM. The specific surface area was calculated assuming that the densities of both nanoparticles are the same as that of bulk Pt_3Ti, 18 g cm^{-3}. The calculated specific surface area of atomically ordered Pt_3Ti nanoparticles, 9.2 ± 5.7 m^2 g^{-1}, was consistent with the value determined by BET measurements, 4.6 ± 0.8 m^2 g^{-1}, within experimental errors.

The inset of Figure 5 shows the CV profiles of atomically disordered and ordered Pt_3Ti nanoparticles for the oxidation of formic acid. The current density of atomically disordered Pt_3Ti nanoparticles (green curve) monotonically increases on the forward (anodic) sweep from −0.2 to 0.4 V. The profile on the reverse (cathodic) sweep from 0.4 to −0.2 V shows a slight deviation from the forward-sweep profile, resulting in a narrow hysteresis. The current density obtained for atomically ordered Pt_3Ti nanoparticles (red curve) shows a potential dependence that is similar to that of atomically disordered Pt_3Ti nanoparticles but is nearly 10 times that of the disordered nanoparticles (note the difference in current scales).

The green and red dashed curves in the inset of Figure 5 represent the blank tests for atomically disordered and ordered Pt_3Ti nanoparticles, respectively, which were obtained in a 0.1 M sulfuric acid solution without formic acid. Each of the blank-test data was subtracted from the measured current density with formic acid to obtain the intrinsic current density, which is related only to the electrochemical oxidation of the fuel. The main panel of Figure 5 shows the CV profiles of atomically disordered and ordered Pt_3Ti nanoparticles together with those of pure Pt and Pt−Ru nanoparticles. The onset potentials of both atomically disordered ($V_{onset} = -0.17$ V) and ordered Pt_3Ti nanoparticles ($V_{onset} = -0.15$ V) are lower than those of either pure Pt ($V_{onset} = -0.09$ V) or Pt−Ru ($V_{onset} = +0.20$ V) nanoparticles. The current density of atomically ordered Pt_3Ti is much higher than that of atomically disordered Pt_3Ti, pure Pt, or Pt−Ru nanoparticles (see Table 1).

The inset of Figure 6 shows the CV profiles of atomically disordered and ordered Pt_3Ti nanoparticles for methanol oxidation. The current density for atomically disordered Pt_3Ti nanoparticles (green curve) steeply rises near 0.1 V on the forward (anodic) sweep from −0.2 to 0.65 V. The reverse-sweep (cathodic) profile shows a wide hysteresis relative to the forward-sweep profile below 0.3 V. The current density of atomically ordered Pt_3Ti nanoparticles (red curve) shows a potential dependence similar to that of atomically disordered Pt_3Ti nanoparticles. The current density of atomically ordered Pt_3Ti nanoparticles is, however, substantially higher relative to that of atomically disordered Pt_3Ti nanoparticles.

The main panel of Figure 6 shows the CV profiles of atomically disordered and ordered Pt_3Ti nanoparticles together with those of pure Pt and Pt−Ru nanoparticles. As before, the blank-test data are subtracted from the measured current

Table 1. Onset potentials and intrinsic current densities at various potentials for pure Pt, Pt−Ru, atomically disordered Pt_3Ti, and atomically ordered Pt_3Ti nanoparticles for the formic acid oxidation

	onset potential (V vs Ag/AgCl)	current density (mA cm^{-2}) @ specified potentials			
		−0.1 V	0.0 V	0.1 V	0.2 V
Pure Pt	−0.09	0.002	0.008	0.018	0.033
Pt−Ru	+0.20	−0.002	0.001	0.002	0.009
disordered Pt_3Ti	−0.17	0.015 ± 0.002	0.036 ± 0.005	0.061 ± 0.008	0.089 ± 0.012
ordered Pt_3Ti	−0.15	0.11 ± 0.07	0.27 ± 0.17	0.45 ± 0.28	0.61 ± 0.38

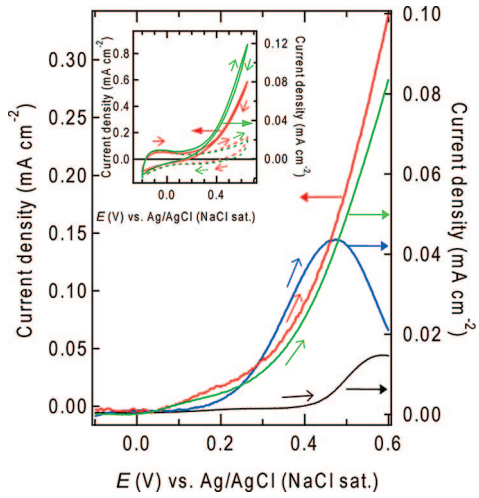

Figure 6. Full curves in the inset represent the CV profiles of atomically disordered (green) and ordered (red) Pt_3Ti nanoparticles for methanol oxidation. Dashed curves in the inset represent the profiles of the blank test for atomically disordered (green) and ordered (red) Pt_3Ti nanoparticles. The green and red curves correspond to the right and left axes of the inset, respectively. The green, red, black, and blue curves on the main panel represent the intrinsic current densities of atomically disordered Pt_3Ti, atomically ordered Pt_3Ti, pure Pt, and Pt−Ru nanoparticles, respectively, for the oxidation of methanol.

densities. The onset potentials of both atomically disordered and ordered Pt_3Ti nanoparticles for methanol oxidation, V_{onset} = +0.04 V and +0.05 V, respectively, are lower than those of either pure Pt (V_{onset} = +0.40 V) or Pt−Ru (V_{onset} = +0.14 V) nanoparticles. The current density of atomically ordered Pt_3Ti nanoparticles is much higher than that of atomically disordered Pt_3Ti, pure Pt, or Pt−Ru nanoparticles (see Table 2).

We conclude that both atomically disordered and ordered Pt_3Ti nanoparticles have higher electrocatalytic activity toward both formic acid and methanol than either pure Pt or Pt−Ru nanoparticles in terms of the low onset potentials. Moreover, the current densities of atomically ordered Pt_3Ti nanoparticles for the oxidation of both formic acid and methanol are substantially higher than those of pure Pt, Pt−Ru, or atomically disordered Pt_3Ti nanoparticles.

CV measurements have been performed on the Pt_3Ti nanoparticles with different particle sizes to explore the relation between the particle size and activity of the catalyst. Figure 7 shows the current densities, j, of the Pt_3Ti nanoparticles with different particle sizes, d, for the oxidation of methanol. The measured CV currents were converted into j using d values obtained from pXRD. The Pt_3Ti nanoparticles with d = 11, 23, and 35 nm were obtained by annealing the as-prepared product (with d = 3 nm) at T = 400, 500, and 600 °C, respectively.

With increasing d from 3 nm, j shows maxima near d = 23 nm for all the measurement potentials of +0.2, +0.4, and +0.6 V. Note that the Pt_3Ti nanoparticles with d = 23 nm show a higher j than that of the larger Pt_3Ti nanoparticles with d = 35 nm. This behavior is not consistent with the expectation based on the mass-transfer effect that the larger catalyst particles will show higher apparent current densities than the smaller catalyst particles due to higher reactant mass transfer to the catalyst surface. The mass-transfer effect is, therefore, not likely to be the major factor for the high electrocatalytic activity of atomically ordered Pt_3Ti nanoparticles. Instead, it is necessary to take into account the particle size effect[29] and/or the effect of the structural transition from the disordered FCC-type to the ordered Cu_3Au-type structures, which can affect the electronic structure of the Pt_3Ti nanoparticles.

It is not possible to separately evaluate the particle size effect and the effect of the structural transition at this stage, since both the particle size and the degree of structural order are dependent on the annealing temperature, T. We intend to synthesize atomically ordered and disordered Pt_3Ti nanoparticles with the same particle size and perform electrochemical measurements on them to assess the effect of the structural transition on the electrocatalytic activity of the Pt_3Ti nanoparticles.

Figure 8 shows the CO stripping profiles of pure Pt, Pt−Ru, atomically disordered Pt_3Ti, and atomically ordered Pt_3Ti nanoparticles. The current densities of pure Pt nanoparticles are presented in Figure 8a as functions of potentials before (i_{before}: dashed curves) and after (i_{after}: full curves) CO exposure. On the forward (anodic) sweep from −0.2 to 0.5 V, the i_{after} is suppressed to nearly zero relative to the i_{before} due to the strong passivation of the catalyst surface by irreversible adsorption of CO. The CO admolecules are stripped from the catalyst surface by raising the potential beyond 0.5 V. The strong CO stripping peaks at 0.5 V and beyond indicate that pure Pt nanoparticles adsorb a large amount of CO as a result of the high affinity of Pt surfaces toward CO adsorption. Figure 8b shows the CO stripping profiles of Pt−Ru nanoparticles. Similarly to the i_{after} of pure Pt nanoparticles, the i_{after} of Pt−Ru nanoparticles is suppressed to nearly zero relative to the i_{before} on the forward (anodic) sweep from −0.2 to 0.1 V. The i_{after} rises at 0.1 V and shows a strong CO stripping peak near 0.3 V. The substantial change in the CV profiles of Pt−Ru nanoparticles before and after CO exposure demonstrates that Pt−Ru nanoparticles have a high affinity toward CO adsorption.[30]

The CO stripping profiles of atomically disordered Pt_3Ti nanoparticles are presented in Figure 8c. On the forward sweep from −0.2 V, the i_{after} steeply increases to reach a valley at 0.1 V via a hump at −0.05 V. The i_{after} grows from 0.1 to 0.65 V, showing a shoulder at 0.5 V. The hump of the i_{after} is slightly diminished relative to that of the i_{before}, which is ascribed to the passivation of the catalyst surface by CO adsorption. The shoulder in the i_{after} is ascribed to the CO stripping peak by analogy to the pure Pt nanoparticles. The CO stripping peak is much weaker than that of either pure Pt or Pt−Ru nanoparticles, which indicates that atomically disordered Pt_3Ti nanoparticles have a much lower affinity toward CO adsorption than either pure Pt or Pt−Ru nanoparticles.

Table 2. Onset potentials and intrinsic current densities at various potentials for pure Pt, Pt−Ru, atomically disordered Pt_3Ti, and atomically ordered Pt_3Ti nanoparticles for the methanol oxidation.

	onset potential (V vs Ag/AgCl)	current density (mA cm^{-2}) @ specified potentials			
		0.0 V	0.2 V	0.4 V	0.6 V
Pure Pt	+0.40	0.000	0.001	0.002	0.015
Pt−Ru	+0.14	0.001	0.004	0.036	0.021
disordered Pt_3Ti	+0.04	0.000	0.005± 0.001	0.024 ± 0.003	0.084± 0.011
ordered Pt_3Ti	+0.05	−0.004 ±0.002	0.016 ± 0.010	0.089 ±0.056	0.34 ± 0.21

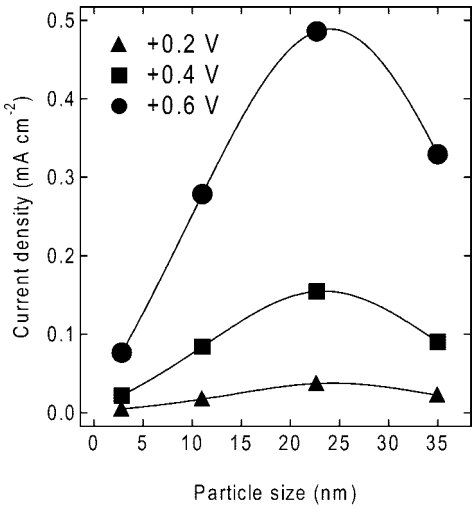

Figure 7. Current densities of the Pt_3Ti nanoparticles for the oxidation of methanol, indicated as functions of the particle size. Current densities at the measurement potentials of +0.2, +0.4, and +0.6 V are represented by closed triangles ▲, squares ■, and circles ●, respectively.

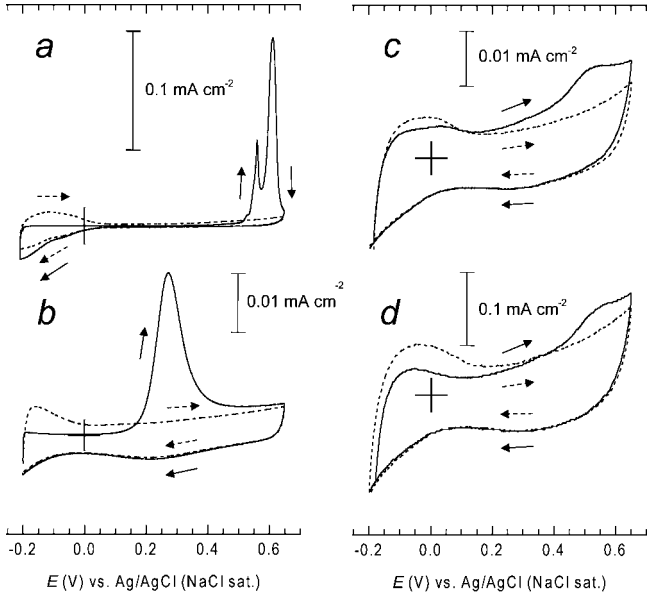

Figure 8. CO stripping profiles of pure Pt (a), Pt−Ru (8b), atomically disordered Pt_3Ti (c), and atomically ordered Pt_3Ti (d) nanoparticles. The dashed and full curves correspond to the CV data before and after CO exposure, respectively.

Figure 8d shows the CO stripping profiles of atomically ordered Pt_3Ti nanoparticles. Similarly to atomically disordered Pt_3Ti nanoparticles, atomically ordered Pt_3Ti nanoparticles show a CO stripping peak at 0.5 V. The CO stripping peak of atomically ordered Pt_3Ti nanoparticles is somewhat weaker than that of atomically disordered Pt_3Ti nanoparticles and much weaker than that of either pure Pt or Pt−Ru nanoparticles. We conclude that both atomically disordered and ordered Pt_3Ti nanoparticles have a much lower affinity toward CO adsorption than either pure Pt or Pt−Ru nanoparticles. We are planning experiments using differential electrochemical mass spectroscopy (DEMS) to explore the generation of CO on Pt_3Ti nanoparticles during fuel oxidation.

In conclusion, we have demonstrated a coreduction strategy for the preparation of Pt_3Ti in the form of nanoparticles. The use of air-free synthetic conditions and organometallic precursors leads to the formation of atomically disordered Pt_3Ti nanoparticles with a particle size of 3 ± 0.4 nm at room temperature. Atomically ordered Pt_3Ti nanoparticles with a particle size of 37 ± 23 nm were obtained by annealing atomically disordered Pt_3Ti nanoparticles in vacuum at 600 °C. Furthermore, we have shown that both atomically disordered and ordered Pt_3Ti nanoparticles have a higher electrocatalytic performance than conventional electrocatalysts in terms of their low onset potentials for fuel oxidation and low affinity toward CO adsorption. In particular, atomically ordered Pt_3Ti nanoparticles demonstrate a promising performance as anode catalysts for direct fuel cells. The large particle size of atomically ordered Pt_3Ti nanoparticles limits the figure of merit of the material for the practical application to direct fuels cells. We will continue to explore ways to induce atomic ordering at temperatures lower than 600 °C and to retain smaller particle sizes, ideally, 3 to 5 nm. The high electrocatalytic performance of atomically ordered Pt_3Ti nanoparticles shows that Pt-based intermetallic compounds containing early *d*-metal elements, Zr, Hf, V, Nb, or Ta, are worthy of further study.

Acknowledgment. This work was supported by the Basic Energy Sciences Division of the Department of Energy through Grant No. DE-FG02 87ER45298. This work was carried out at the UHV-STEM Laboratory of the Cornell Center for Materials Research (CCMR) with support from program Grant No. DMR 05204040 from the National Science Foundation Materials Research Science and Engineering Centers (MRSEC). The authors would like to thank Malcolm Thomas for help with the STEM images, the CBED patterns, and the EDS data. The authors also would like to thank Dr. Eiji Abe of the University of Tokyo for the fruitful discussions on the CBED patterns.

JA075061C

(29) Frelink, T.; Visscher, W.; van Veen, J. A. R. *J. Electroanal. Chem.* **1995**, *382*, 65–72.
(30) Maillard, F.; Lu, G. -Q.; Wieckowski, A.; Stimmung, U. *J. Phys. Chem. B* **2005**, *109*, 16230–16234.